MSDE

ROYAL SOCIETY OF CHEMISTRY

COMMUNICATION

View Article Online
View Journal | View Issue

Cite this: *Mol. Syst. Des. Eng.*, 2020, 5, 97

Received 12th August 2019,
Accepted 2nd December 2019

DOI: 10.1039/c9me00104b

rsc.li/molecular-engineering

A dehydrobenzoannulene-based two-dimensional covalent organic framework as an anode material for lithium-ion batteries†

Eric R. Wolfson, Neng Xiao, Luke Schkeryantz, W. Karl Haug, Yiying Wu and Psaras L. McGrier *

Developing anode materials with excellent cycling performance and energy capacities for lithium-ion batteries (LIBs) is a challenging task. Herein, we report the synthesis of an imine-linked covalent organic framework (COF) containing redox-active dehydrobenzoannulene (DBA) units. The bulk DBA-COF 3 system exhibits a reversible capacity of 207 mA h g^{-1} at 50 mA g^{-1} after 90 cycles. This work highlights the potential of utilizing DBA units to construct efficient organic-based anode materials for LIBs.

Design, System, Application

The effects of global warming and rising sea levels on the planet has led to an increased effort of moving beyond fossil fuels as a primary source of energy. In its place, technologies utilizing renewable resources such as wind and solar energies have emerged, and as a result the demand for more efficient forms of energy storage has risen substantially. Lithium-ion batteries (LIBs) have become a popular method of energy storage whose continued development is dependent upon finding new anode materials that can rival the performance of graphite. The use of covalent organic frameworks (COFs), a crystalline class of porous polymers, offers a potential solution thanks to their high surface areas and modular structures, which enables the integration of a wide variety of redox-active frameworks suitable for energy storage applications. In this work, an imine-linked COF is synthesized using redox-active dehydrobenzoannulene (DBA) units and investigated as a novel anode material for LIBs. Since the electronic properties of COFs can be tuned by the careful selection of redox-active monomers, this work highlights a rare example of how porous polymer-based anode materials can be engineered by designing and incorporating novel redox-active building blocks with redox potentials below 2 V.

Introduction

Global interest in more environmentally benign forms of energy production has led to an increasing demand for high-performance energy storage devices. Lithium ion batteries (LIBs) represent an important class of energy storage devices because they can simultaneously provide high energy capacities and high power outputs, which is desirable for portable electronics and electric vehicles.[1,2] However, the performance of LIBs is highly dependent on the efficiency of the anode. Graphite, the current industrial anode material for LIBs, offers a maximum theoretical capacity of 372 mA h g^{-1} but the experimental rate performance provides capacities that are much lower. Although inorganic-based anodes containing Si,[3] Sn,[4] and Ge[5] have exhibited reversible capacities higher than 1000 mA h g^{-1}, they often undergo volume expansion during the insertion/extraction of Li ions which leads to "dead" isolated areas that compromise the cycling performance of the materials. Thus, there is an on-going challenge to produce low-cost anode materials that exhibit high energy capacities and great cycling performance.

Covalent organic frameworks (COFs),[6] a crystalline class of porous polymers, have emerged as a suitable platform to construct lightweight organic-based electrodes for LIBs thanks to their low densities, high surface areas, tunable pore sizes, and great chemical stability. These features have also been exploited for applications in catalysis,[7,8] energy storage,[9–11] proton conduction,[12,13] and spintronics.[14] COFs enable the integration of various π-electron conjugated monomers to construct two-dimensional (2D) materials with tailored redox properties. For instance, Feng, Wang, and co-workers have shown[15] that an exfoliated COF containing redox-active anthraquinone units exhibited fast diffusion of Li ions and specific capacities as high as 210 mA h g^{-1}. Recently, Li and co-workers have demonstrated[16] that a poly(imide-benzoquinone)-based COF assembled on graphene exhibited a reversible capacity of 271 mA h g^{-1}. While these examples highlight the benefits of utilizing COFs to create high-performance electrode materials with efficient Li ion diffusion and electron transport properties, they mostly apply to organic-based cathodes because their redox potentials are between 2.0–4.0 V *versus* Li/Li^+.[17] Examples of COF-based anodes for LIBs are rare with the lone exception of a 14-electron redox-active imine-linked COF system recently

Department of Chemistry & Biochemistry, The Ohio State University, Columbus, Ohio 43210, USA. E-mail: mcgrier.1@osu.edu

† Electronic supplementary information (ESI) available: Synthetic procedures, FT-IR, solid-state ^{13}C NMR, TGA, PXRD, and SEM. See DOI: 10.1039/c9me00104b

reported by Sun, Wang, and co-workers.[18] As a consequence, finding redox-active monomers that can be utilized to construct cheap organic-based anode materials that could potentially rival graphite is highly desirable.

Herein, we report the synthesis, characterization, and electronic properties of an imine-linked 2D COF containing dehydrobenzoannulene (DBA)[19–21] units. DBAs are π-conjugated triangular shaped macrocycles that exhibit reversible redox potentials[22] and the ability to use their soft alkynyl ligands to bind Li.[23,24] We show that **DBA-COF 3** exhibits a reversible capacity of 207 mA h g^{-1} after 90 cycles at 50 mA g^{-1}. Since **DBA-COF 3** exhibits a coulombic efficiency above 95%, this work highlights the potential of utilizing DBA units to construct efficient organic-based anode materials for LIBs.

Results and discussion

DBA-COF 3 was synthesized by reacting DBA[12]-CHO with *para*-phenylenediamine (PPD) in a 19 : 1 (v/v) mixture of *ortho*-dichlorobenzene (*o*-DCB) and *n*-BuOH at 120 °C for 72 h (Scheme 1).

DBA-COF 3 was obtained by filtration and washed excessively with methanol to produce a yellow solid. **DBA-COF 3** was purified by stirring the yellow solids in DMF and methanol for 30 minutes each to remove any unreacted monomers. Afterwards, **DBA-COF 3** was collected by filtration, washed excessively with methanol, and dried under vacuum.

DBA-COF 3 was characterized by Fourier transform infrared spectroscopy (FT-IR) and ^{13}C cross-polarization magic angle spinning (CP-MAS) spectroscopy. The FT-IR spectra revealed a stretching mode at 1614 cm^{-1} (C═N), which is indicative of the imine-linkages (Fig. S1, ESI†). The connectivity of **DBA-COF 3** was confirmed by ^{13}C CP-MAS exhibiting a resonance at 152.8 ppm that corresponds to the carbon on the imine bond, and a resonance at 92.0 ppm, which corresponds to the alkynyl units of DBA[12] (Fig. S3, ESI†).

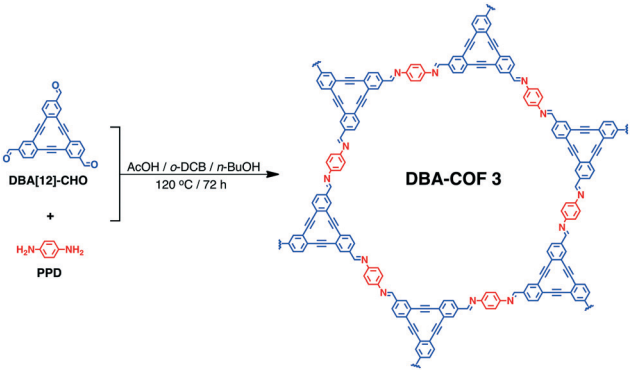

Scheme 1 Synthesis of **DBA-COF 3**.

Thermogravimetric analysis (TGA) indicated that **DBA-COF 3** retained ~95% of its weight up to 555 °C (Fig. S7, ESI†). Scanning electron microscopy (SEM) images revealed a fluffy and cloud-like morphology for the material (Fig. S8, ESI†).

The porosity of **DBA-COF 3** was examined by nitrogen gas adsorption at 77 K (Fig. 1). **DBA-COF 3** exhibited a type IV isotherm displaying a sharp uptake at low pressure (P/P_0 < 0.01) followed by a small step between P/P_0 = 0.18 and 0.30. Application of the Brunauer–Emmett–Teller (BET) model over the low-pressure region (0.13 < P/P_0 < 0.18) provided a surface area of 1244 m^2 g^{-1}. The total pore volume for **DBA-COF 3** calculated at P/P_0 = 0.899 provided a value of 0.58 cm^3 g^{-1}. The pore size distribution of **DBA-COF 3** was estimated using the nonlocal density functional theory (NLDFT) method yielding a value of 2.1 nm. The experimental pore size is lower than the theoretical of 3.3 nm, which is indicative of the stacking layers being significantly offset. However, the large pore size of **DBA-COF 3** is advantageous for diffusion of electrolyte solution and the facilitation of ion transport.

The crystallinity of **DBA-COF 3** was evaluated using powder X-ray diffraction (PXRD). Taking the differences between the experimental and theoretical pore sizes into consideration, **DBA-COF 3** was modeled using a *P*6 hexagonal unit cell in which the adjacent layers were offset by 12 Å (Fig. 2). **DBA-COF 3** displays an intense peak at 3.28° followed by smaller peaks at 5.49°, 6.32°, and 25.7°, which correspond to the (100), (110), (200), and (001) planes, respectively. Pawley refinement of the experimental PXRD data provided unit cell parameters of $a = b$ = 32.265 Å and c = 3.4 Å (residuals R_p = 2.91%, R_{wp} = 3.53%). The simulated patterns were in good agreement with the experimental profile. Stability tests revealed that the crystallinity of **DBA-COF 3** is retained after soaking the material for 24 h in various protic/aprotic solvents and aqueous solutions (Fig. S9, ESI†).

Psaras L. McGrier

Psaras is an Assistant professor in the Department of Chemistry and Biochemistry at The Ohio State University. He received his B.S. in Chemistry from the University of South Carolina–Aiken in 2004 and his Ph.D. in Organic/Polymer chemistry from the Georgia Institute of Technology (Georgia Tech) in 2010 under the direction of Professor Uwe Bunz. After finishing his Ph.D., he moved to Northwestern University (2010–2013) to join the group of Professor Sir Fraser Stoddart as a postdoctoral scholar on a fellowship from Georgia Tech Facilitating Academic Careers in Engineering and Science (FACES) committee and the National Science Foundation (NSF). His current research interests include the synthesis and utilization of 2D and 3D porous polymers for practical applications. He is a recipient of the 2018 ACS Division of Polymeric Materials: Science and Engineering (PMSE) Young Investigator Award.

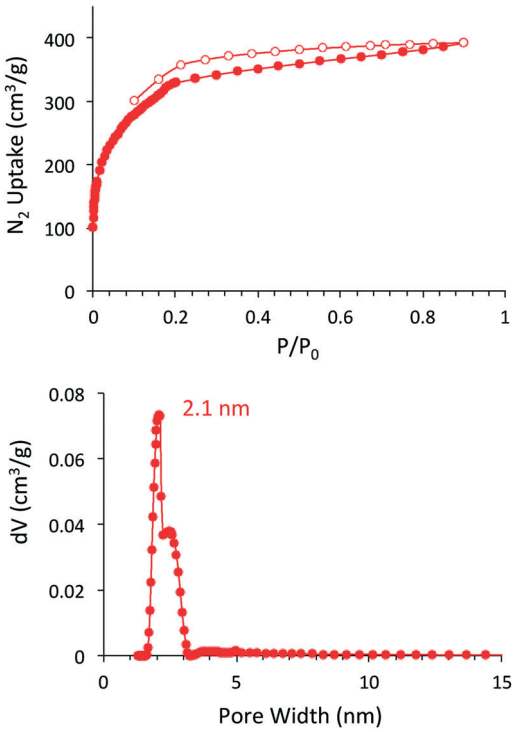

Fig. 1 Nitrogen adsorption/desorption isotherm (top) and NLDFT pore size distribution (bottom) for **DBA-COF 3**.

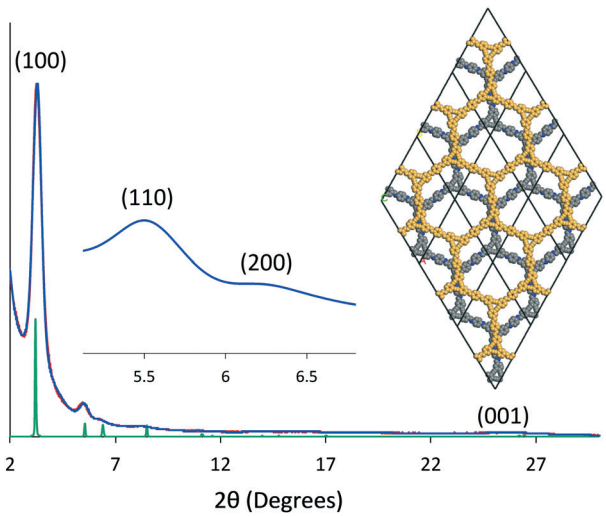

Fig. 2 Indexed experimental (red) and Pawley refined (blue) patterns of **DBA-COF 3** compared to the simulated hexagonal unit cell (green) with an offset of 12 Å.

The electrochemical performance was evaluated by combining **DBA-COF 3** with Super-P conductive carbon and poly(vinylidenefluoride) (PVDF) in a 6 : 3 : 1 ratio using CR2032-type coin cells with metallic Li as the counter electrode. After the second charge/discharge cycle, cyclic voltammetry (CV) data revealed that **DBA-COF 3** exhibits a pair of quasi-reversible redox peaks at 0.79 and 1.18 V (between 0.0 to 3.0 V) with 1 M $LiPF_6$ as the electrolyte in 1 : 1 (v/v) ethylene carbonate (EC) and dimethyl carbonate (DMC)

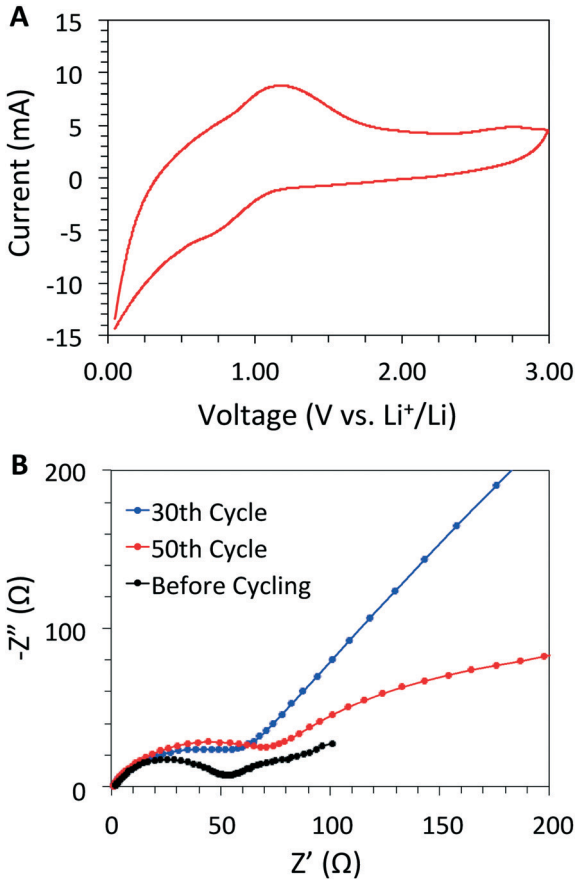

Fig. 3 (A) CV plot of **DBA-COF 3** using 1 M $LiPF_6$ in (1 : 1, v/v) EC/DMC at a scan rate of 10 mV s^{-1}, and (B) an EIS profile of **DBA-COF 3** at 10 mV for different cycles.

(Fig. 3A). The peak current increases linearly in relation to the square root of the sweep rate demonstrating that the redox kinetics for this system are faradaic as opposed to capacitive (Fig. S10, ESI†). The redox process is likely attributed to the sequential lithiation/delithiation of the imine-linkage[18,25] and DBA core. In contrast, DBA[12]-imine, an analog of **DBA-COF 3** (Fig. S12, ESI†), exhibited a trio of redox peaks at 1.28, 1.01, and 0.91 V with 1 M $LiPF_6$ in DMF corresponding to a similar lithiation/delithiation process. The reduction peaks of DBA[12]-imine at 1.01 and 0.91 V appear to merge together in the CV plot of **DBA-COF 3** (Fig. 3A). However, a CV plot of the DBA[12]-H hydrocarbon also exhibits a broad reduction peak at 0.85 V in 1 M $LiPF_6$ in DMF (Fig. S12, ESI†), which suggests that the initial lithiation is possibly occurring on the DBA vertex and not the benzene ring of the PPD linker of **DBA-COF 3**.

To investigate the lithiation/delithiation process, we performed X-ray photoelectron spectroscopy (XPS) on pristine, lithiated, and delithiated coin cells of **DBA-COF 3**. The C 1s region of the pristine coin cell (Fig. S15, ESI†) exhibits five peaks at 290.0, 286.6, 284.8, and 282.9 eV, which correspond to the C═O, C–N, C═C, and C≡C functional groups, respectively. XPS of the lithiated coin cell (Fig. S16, ESI†) revealed the growth of a new peak at 288.4 eV, and a

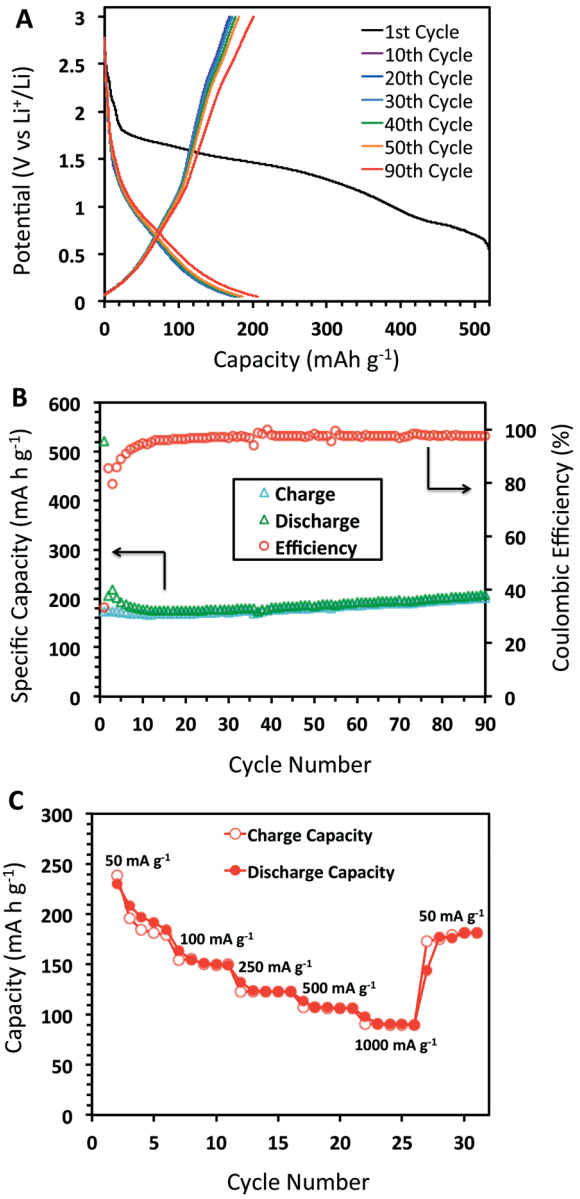

Fig. 4 (A) Charge/discharge profile at 50 mA g^{-1}, (B) cycling performance of **DBA-COF 3** after 90 cycles, and (C) capacities at different charge–discharge rates from 50–1000 mA g^{-1} at 5 cycles each.

significant attenuation of the peak at 282.8 eV, which correspond to the emergence of C–O moieties and a decrease in the number of alkynyl (–C≡C–) substituents, respectively. The former reflects the degradation of electrolyte to form the solid-electrolyte interface (SEI) layer,[26] while the latter is indicative of lithiating the alkynyl units of the DBA core. Delithiation of **DBA-COF 3** notably restores the corresponding alkynyl peak demonstrating reversibility of the Li binding event (Fig. S17, ESI†). While it is known that lithiation/delithiation also occurs at the imine functionalities for similar systems,[18,25] these results demonstrate that lithiation/delithiation of the alkynyl units of the DBA also serve a critical role in the Li-storage mechanism for **DBA-COF 3**.

The charge/discharge curves for **DBA-COF 3** after 90 cycles at 50 mA g^{-1} are provided in Fig. 4A. The first cycle afforded a value of 522 mA h g^{-1} and a low coulombic efficiency of 33.3%. The low efficiency is attributed to the initial formation of the SEI layer due to decomposition of the electrolyte. After the 30th and 50th cycles, **DBA-COF 3** exhibits reversible capacities of 178 and 185 mA h g^{-1} with coulombic efficiencies of 95.1 and 97.9%, respectively (Fig. 4B). Electrochemical impedance spectroscopy (EIS) revealed impedance values of 47.8 Ω after 30 cycles and 66.7 Ω after 50 cycles (Fig. 3B). The emergence of a larger semicircle at the 50th cycle represents a small increase in the charge-transfer resistance of the cell and is attributed to the growth of a passivation layer on **DBA-COF 3**, which leads to an increase in the columbic efficiency of the bulk system. After the 90th cycle, **DBA-COF 3** exhibits an increased reversible capacity of 207 mA h g^{-1} and a steady efficiency of 97.4%. The excellent electrochemical performance of **DBA-COF 3** is attributed to its insolubility in the electrolyte, the structural stability of the framework, and the incorporation of the redox-active DBA units.

In addition, we also investigated the rate performance of **DBA-COF 3** (Fig. 4C). Testing **DBA-COF 3** at increasing current densities of 50, 100, 250, 500, and 1000 mA g^{-1} at five cycles each afforded reversible capacities of 184, 149, 123, 107, and 90 mA h g^{-1}, respectively. Although increasing the current density from 50 to 1000 mA g^{-1} leads to a 50% decrease in performance, the reversible capacity is mostly recovered at 50 mA g^{-1} after 30 cycles with a value of 181 mA h g^{-1}. Overall, this data suggests that **DBA-COF 3** exhibits respectable charge and discharge capabilities at low and high current densities.

Conclusions

In summary, an imine-linked COF containing DBA units was synthesized and utilized as an anode material for LIBs. **DBA-COF 3** exhibited excellent electrochemical performance in the bulk phase yielding a reversible capacity of 207 mA h g^{-1} and a coulombic efficiency of 97.4% after 90 cycles. This work highlights the rare example of utilizing DBA units to construct lightweight COF-based electrodes with high surface areas for LIBs. The low redox potentials of DBAs makes them suitable for constructing the next generation of organic-based anode materials with excellent cycling performance and high-energy capacities.

Conflicts of interest

There are no conflicts to declare.

Acknowledgements

P. L. M. acknowledges the National Science Foundation (NSF) and Georgia Tech Facilitating Academic Careers in Engineering and Science (GT-FACES) for a Career Initiation Grant. We acknowledge The Ohio State University Campus

Chemical Instrument Center (CCIC) and Tanya Whitmer for assistance with the CP-MAS NMR measurements and access to the instrumentation.

References

1 J. B. Goodenough and Y. Kim, *Chem. Mater.*, 2010, **22**, 587–603.
2 B. Dunn, H. Kamath and J.-M. Tarascon, *Science*, 2011, **334**, 928–935.
3 M. T. Demirkan, L. Trahey and T. Karabacak, *J. Power Sources*, 2015, **273**, 52–61.
4 P. Meduri, C. Pendyala, V. Kumar, G. U. Sumansekera and M. K. Sunkara, *Nano Lett.*, 2009, **9**, 612–616.
5 C. K. Chan, X. F. Zhang and Y. Cui, *Nano Lett.*, 2008, **8**, 307–309.
6 R. P. Bisbey and W. R. Dichtel, *ACS Cent. Sci.*, 2017, **3**, 533–543.
7 Q. Fang, S. Gu, J. Zheng, Z. Zhuang, S. Qui and Y. Yan, *Angew. Chem., Int. Ed.*, 2014, **53**, 2878–2882.
8 J. Zhang, X. Han, X. Wu, Y. Liu and Y. Cui, *J. Am. Chem. Soc.*, 2017, **139**, 8277–8285.
9 C. R. Deblase, K. E. Silberstein, T. T. Truong, H. D. Abruña and W. R. Dichtel, *J. Am. Chem. Soc.*, 2014, **135**, 16821–16824.
10 C. Mulzer, L. Shen, R. P. Bisbey, J. R. McKone, N. Zhang, H. D. Abruña and W. R. Dichtel, *ACS Cent. Sci.*, 2016, **2**, 667–673.
11 S. Chandra, D. R. Chowdhury, M. Addicoat, T. Heine, A. Paul and R. Banerjee, *Chem. Mater.*, 2017, **29**, 2074–2080.
12 S. Chandra, T. Kundu, S. Kandambeth, R. BabaRao, Y. Marathe, S. M. Kunjir and R. Banerjee, *J. Am. Chem. Soc.*, 2014, **136**, 6570–6573.
13 H. Xu, S. Tao and D. Jiang, *Nat. Mater.*, 2016, **15**, 722–726.
14 E. Jin, M. Asada, Q. Xu, S. Dalapati, M. A. Addicoat, M. A. Brady, H. Xu, T. Nakamura, T. Heine, Q. Chen and D. Jiang, *Science*, 2017, **357**, 673–676.
15 S. Wang, Q. Wang, P. Shao, Y. Han, X. Gao, L. Ma, S. Yuan, X. Ma, J. Zhou, X. Feng and B. Wang, *J. Am. Chem. Soc.*, 2017, **139**, 4258–4261.
16 Z. Luo, L. Liu, J. Ning, K. Lei, Y. Lu, F. Li and J. Chen, *Angew. Chem., Int. Ed.*, 2018, **57**, 9443–9446.
17 Y. Wang, Y. Deng, Q. Qu, X. Zheng, J. Zhang, G. Liu, V. S. Battaglia and H. Zheng, *ACS Energy Lett.*, 2017, **2**, 2140–2148.
18 Z. Lei, Q. Yang, Y. Xu, S. Guo, W. Sun, H. Liu, L.-P. Lv, Y. Zhang and Y. Wang, *Nat. Commun.*, 2018, **9**, 576.
19 E. L. Spitler, C. A. Johnson II and M. M. Haley, *Chem. Rev.*, 2006, **106**, 5344–5386.
20 J. W. Crowe, L. A. Baldwin and P. L. McGrier, *J. Am. Chem. Soc.*, 2016, **138**, 10120–10123.
21 L. A. Baldwin, J. W. Crowe, D. A. Pyles and P. L. McGrier, *J. Am. Chem. Soc.*, 2016, **138**, 15134–15137.
22 K. Tahara, H. Kozuma, V. Venkatesh, E. Ryomura, H. Miyoshi, K. Nakamachi, R. Kishi, H. Takahashi, M. Nakano and Y. Tobe, *ChemPlusChem*, 2017, **82**, 1052–1056.
23 H. Zhang, M. Zhao, X. He, Z. Wang, X. Zhang and X. Liu, *J. Phys. Chem. C*, 2011, **115**, 8845–8850.
24 H. J. Hwang, J. Koo, M. Park, N. Park, Y. Kwon and H. Lee, *J. Phys. Chem. C*, 2013, **117**, 6919–6923.
25 Z. Man, P. Li, D. Zhou, R. Zang, S. Wang, P. Li, S. Liu, X. Li, Y. Wu, X. Liang and G. Wang, *J. Mater. Chem. A*, 2019, **7**, 2368–2375.
26 N. Schulz, R. Hausbrand, C. Wittich, L. Dimesso and W. Jaegermann, *J. Electrochem. Soc.*, 2018, **165**, A833–A846.